

High-strain, high-strain-rate flow and failure in PTFE/Al/W granular composites

J. Cai^a, S.M. Walley^b, R.J.A. Hunt^b, W.G. Proud^b, V.F. Nesterenko^a, M.A. Meyers^{a,*}

^a Department of Mechanical and Aerospace Engineering, University of California, San Diego, La Jolla, CA 92093-0411, USA

^b Cavendish Laboratory, University of Cambridge, Cambridge CB3 0HE, UK

Received 20 January 2007; received in revised form 8 March 2007; accepted 15 March 2007

Abstract

Dynamic compression experiments were performed on a pressed PTFE/Al/W mixture to understand the composite behavior at high-strain and high-strain rate. The high-strain-rate tests were carried out in a drop-weight apparatus at impact velocities of 3.5 and 5 m/s, providing strain rates of approximately $4 \times 10^2 \text{ s}^{-1}$. Aluminum jackets of varying thickness were used to ensure that specimens underwent confined deformation but did not separate into fragments. Failure was preceded by extensive plastic deformation concentrated primarily in the PTFE component. W particle–PTFE interface separation provided initiation and propagation of cracks. In extensively deformed specimens (strains of up to -0.875), PTFE nanofibers formed along cracks as a result of shear localization and significant softening caused by plastic deformation. The Zerilli–Armstrong constitutive equation for polymeric solids was used to simulate the response of the composite. Its use is justified by the fact that the majority of plastic strain is concentrated in the PTFE polymer.

© 2007 Elsevier B.V. All rights reserved.

Keywords: Drop-weight; High-strain; High-strain-rate deformation; PTFE; Al; W; Polymer composites

1. Introduction

Non-detonating reactive materials are being intensively studied for projectile applications in military operations in urban terrain (MOUT). The requirements are a high density and exothermic reaction initiation upon impact. This paper is concerned with PTFE/Al/W granular materials that underwent high-strain, high-strain-rate deformation in drop-weight tests. The primary function of W is to increase the density of the mixture and for low collateral damage, although it may also participate in the exothermic reactions with Al. Al and PTFE are known to react exothermically [1]. While granular materials are widespread, extensive research on their physics just started a few decades and the properties of complex granular materials remain unexplored so far. The considerable interest in granular materials is due to phenomena they exhibit in applications: segregation, fluidization, stress propagation, etc. [2–4]. For granular powder mixtures, the primary focus is on the kinetics of chemical reactions. Two classes of reactions were proposed by

Thadhani [5] to explain the dynamic effects: shock-assisted reactions have been defined as those occurring in the time scale of thermal equilibration (tens of microseconds to milliseconds), while shock-induced reactions are those occurring in the time scale of pressure equilibration (nano- to micro-second duration) in shock-loading. Meyers et al. [6] and Vecchio et al. [7] investigated Mo–Si and Nb–Si mixtures subjected to shock compression and proposed a mechanism for reaction initiation. This shock reaction was modeled by Eakins et al. [8].

The dynamic properties and shock behavior of a few polymers, such as PTFE, EstaneTM, Kel-F-800TM, polychloroprene, PMMA and epoxy resin, have been investigated to serve as the binder materials [9–12]. PTFE and Kel-F-800TM exhibited constant shear strength behind the shock front, while other polymeric systems showed increased shear strength, a characteristic attributed to the viscoelastic/viscoplastic properties. The shear strengths of PTFE and estaneTM increased with the increase of impact stress, while that of Kel-F-800TM had a constant strength. Teflon (PTFE) was also studied as an inert granular material under dynamic compaction [13] and explosive loading [14,15].

PTFE is an outstanding candidate as the binder material due to a favorable combination of properties: low friction coefficient, high thermal stability, high electrical resistance, high

* Corresponding author. Tel.: +1 858 534 4719; fax: +1 858 534 5698.

E-mail address: mameyers@ucsd.edu (M.A. Meyers).

chemical inertness, high melting point (327°C), high thermal energy release when decomposed, and the easiness to deform. Experiments show that the addition of PTFE into Ti/Si mixture and $\text{Fe}_2\text{O}_3/\text{Al}$ mixture increased the magnitude of reaction and decreased the reaction time [16].

The purpose of this research is to investigate mechanical response, including fracture mechanism, of a PTFE/Al/W mixture under high-strain and high-strain-rate flow. Therefore, the drop-weight technique was adopted, since the weight has sufficient energy to subject the specimens to large strains. This technique was used in the investigation of high-strain-rate deformation behavior of polymers [17] and thermites [18], and in the sensitivity testing of explosive substances [19].

2. Experimental techniques

The PTFE/Al/W composite was fabricated by cold uniaxial pressing at a pressure of 100 MPa. The initial powders had the following average sizes: Al: 2 and 95 μm (ValimeH-2 and H-95); W: 44 μm (Teledyne, –325 mesh); PTFE: 100 nm (DuPont, PTFE 9002-84-0, type MP 1500J).

The mixture had the following weight content of components: 77 wt% W, 17.5 wt% PTFE, and 5.5 wt% Al. The final density of the pressed mixture was 95% of the theoretical density. Due to the large difference in density between the constituents, PTFE was the major component on a volume fraction, 56%, followed by Al, 23% and W, 21%.

The drop-weight test apparatus at the Physics of Solids Group, Cavendish Laboratory [17,20], was used. The schematic of the apparatus is shown in Fig. 1; the specimen was mounted in a sample holder that ensured the parallelism of impact. The velocity of the drop-weight decreases as a function of time after impact.

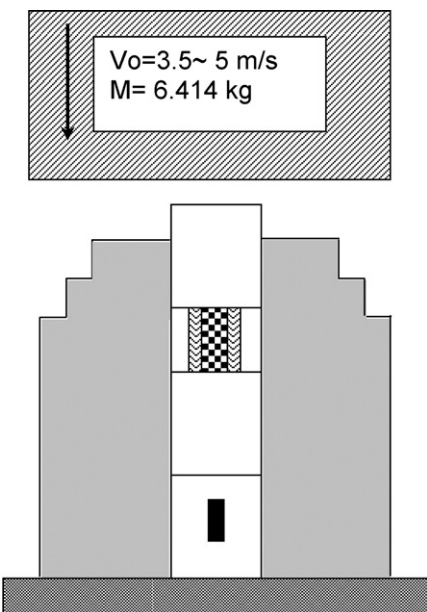


Fig. 1. Schematic drawing of the experimental set-up for drop-weight test. \blacksquare , PTFE/Al/W mixture specimen; \square , confinement Al ring; \blacksquare , sample holder for optimum alignment; \blacksquare , drop weight; \blacksquare , strain gage.

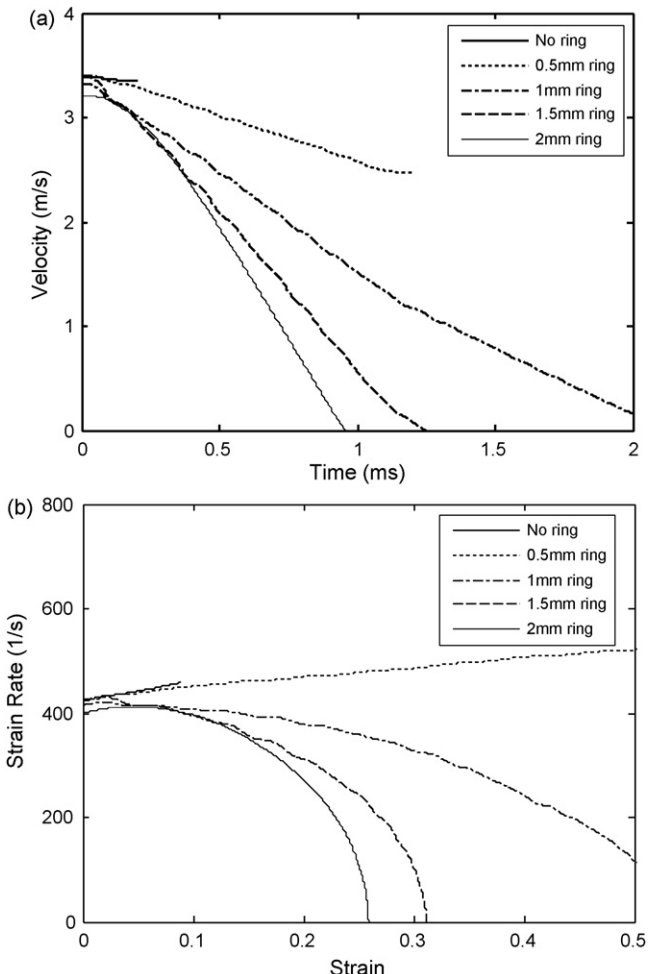


Fig. 2. Effects of confinement on drop-weight velocity and composite deformation strain rate: (a) velocity as a function of time after impact; (b) strain rate as the function of strain.

The specimens were tested in the unconfined and confined conditions. The use of confinement rings of an aluminum alloy 7075-T6 enabled arrest of the experiment at different strains. Aluminum rings with the same height as the specimens and thicknesses of 0.5, 1, 1.5, and 2 mm were used.

The impact velocities were 3.5 and 5 m/s; these two velocities correspond to the drop-weight being released from the standard height of 0.6 m or from the top (1 m high) of the apparatus (Fig. 1). Fig. 2(a) shows the velocities of the drop-weight as a function of time for the 0.6 m set-up; it can be seen that the greater the load, due to the presence of the confinement ring, the faster the velocity decreases. The corresponding strain rates are shown in Fig. 2(b) as a function of strain. For the unconfined specimen and specimen confined with a 0.5 mm ring, the strain rate actually increased slightly from an initial value of approximately 400 s^{-1} . As the Al alloy confinement ring thickness increased, the strain rate decreased. For the 2 mm confinement ring, the strain rate reached zero at a strain of 0.25. This corresponds to the arrest of sample deformation.

The voltage-time trace obtained from the gage below the specimen (Fig. 1) can be converted into a stress by applying a conversion coefficient. The velocity of the drop-weight was

measured and this was used for the determination of the strain. In this manner it was possible to obtain the stress-strain response of the specimen/confinement ring assembly. The procedures are standard and therefore will not be presented here.

For photography, an AWRE C4 rotating-mirror camera was used [21]. It has 140 framing lenses, giving a total recording time of approximately 1 ms. The records were used to probe the localization of failure in unconfined specimens.

3. Results and discussion

3.1. Initial microstructure

The initial microstructure of the composite is shown in Fig. 3. The backscattered image shows the W particles as bright features because of their high atomic number. The Al and PTFE cannot be distinguished in the low-magnification SEM micrograph of

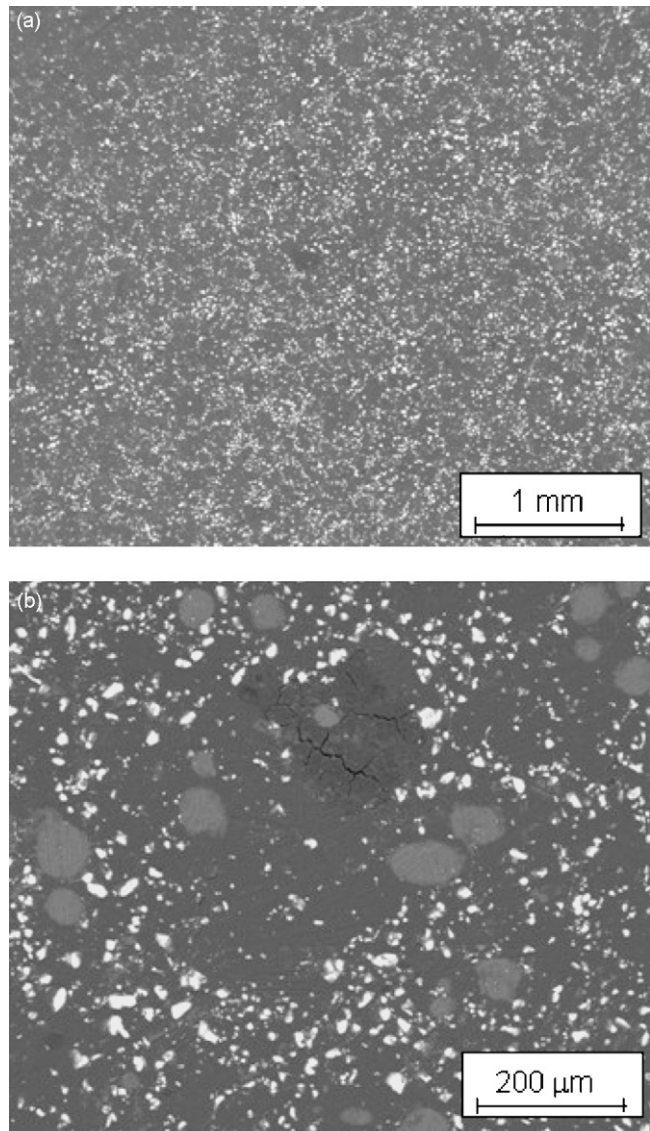


Fig. 3. Backscattered SEM images of initial compact configuration at: (a) lower magnification; (b) higher magnification.

Fig. 3(a) but (b) resolves the features. Medium grey spherical features represent Al agglomerates. The individual Al particles (2 μm diameter) can only be faintly resolved. Observation of a fracture surface shows the three constituents in a clearer fashion (Fig. 4(a)). The larger W particles, which have a spheroidal shape, are surrounded by PTFE (the majority volume fraction) and Al. The PTFE forms the continuous matrix in which the W and Al particles are discretely distributed. Elemental analysis (Fig. 4(b,c, and d)) for three particles is attached.

3.2. Mechanical testing

The different specimens after deformation are shown in Fig. 5. The specimen and an Al confinement ring are shown on top, and the post-deformation configurations at the bottom. As the confinement ring thickness increased the total deformation undergone by specimens decreased, in accordance with the strain rate versus strain plot of Fig. 3(b). The 0.5 mm ring underwent total buckling and folding, whereas the 1mm ring underwent barreling and lateral cracking. On the other hand, the 1.5 and 2 mm rings retained their cylindrical shape. The aluminum ring (2 mm thick) was tested separately both quasistatically and dynamically. The results are shown in Fig. 6. By comparison, the quasistatic compression curve (10^{-3} s^{-1}) is much more smooth and accurate. The results in Fig. 6 indicate that the dynamic strength of the aluminum alloy used is approximately 400 MPa, whereas the quasistatic strength is approximately 300 MPa. It can be assumed that the strength of the material reaches a saturation level where work hardening is absent. This strain-rate sensitivity is expected in aluminum alloys [22–24]. This value was used in estimating the corrected flow stresses of the specimen-confinement assemblies.

It should be mentioned that the Al rings only provide limited confinement since the internal diameter of the rings increases with strain. In the absence of frictional stresses at the platens, the volume inside the orifice is constant. Thus, the principal effects of the Al rings are (a) to allow the specimen to deform without fragment, and (b) to provide a limited confinement.

The results of the dynamic tests under different confinement conditions are shown in Fig. 7. In the absence of confinement the stress rises to 60 MPa and rapidly drops (Fig. 7(a)). This is due to fracture and fragmentation of the specimen under the anvil. This occurs at a low strain of 0.035. The confinement significantly increases the range of plastic strain that the specimens can undergo, as shown in Fig. 7(b–d). The fluctuations in stress are very high. For the 0.5 mm Al ring, the flow stress is approximately 80 MPa, slightly higher than the unconfined specimen. However, the specimen retains its load-carrying ability up to a strain of 0.5. As the thickness of the confinement ring increases to 1 and 1.5 mm, the strength of the composite increases correspondingly. This is evidence of confinement, which is actually non-existent if one assumes that frictional effects at the platens do not exist.

The calculated stress-strain response obtained from the Zerilli–Armstrong constitutive equation [25] for polymeric materials is shown in Fig. 8. The equation was inspired in the two Z–A equations for metals [26,27]. The constitutive model

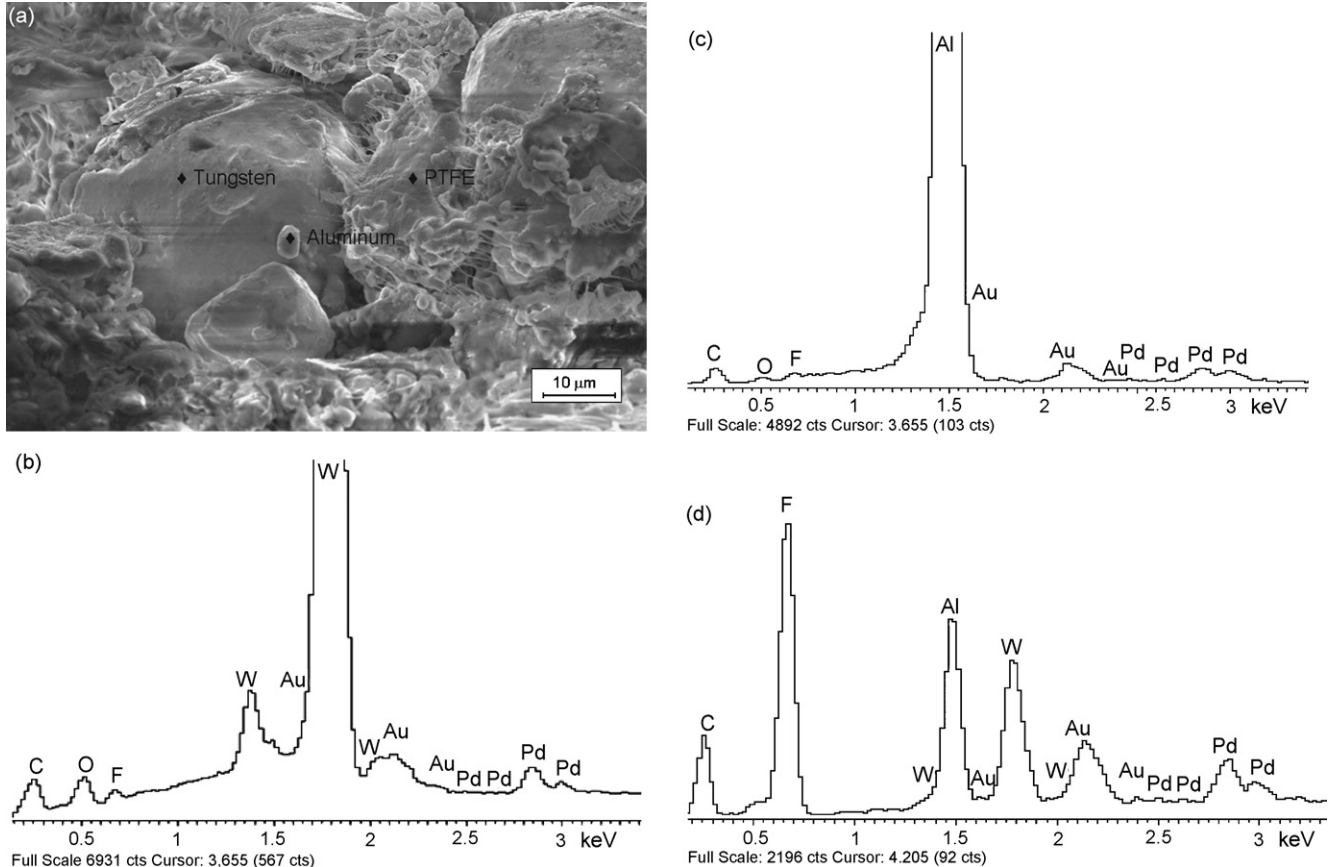


Fig. 4. Identification of three components by secondary SEM and EDS: (a) fracture surface; (b) W; (c) Al; (d) PTFE.

has the form:

$$\sigma = B e^{-\beta T} + B_0 \sqrt{\frac{(1 - e^{-\omega \varepsilon})}{\omega e^{-\alpha T}}}$$

where

$$\begin{aligned} \beta &= \beta_0 - \beta_1 \ln \dot{\varepsilon}, & \alpha &= \alpha_0 - \alpha_1 \ln \dot{\varepsilon}, \\ \omega &= \omega_a + \omega_b \ln \dot{\varepsilon} + \omega_p p, & B &= B_{pa}(1 + B_{pb}p)^{B_{pm}}, \\ B_0 &= B_{0pa}(1 + B_{0pb}p)^{B_{0pm}} \end{aligned}$$

where T is the temperature, P the pressure, $\dot{\varepsilon}$ the strain rate and the other symbols are parameters listed in Table 1. Fig. 8(a) shows the calculated stress-strain response for PTFE compared to the experimental results by Walley et al. [17]. Fig. 8(b) shows the predicted values of the flow stress (for strain = 0.04) as well as the experimental values for the PTFE/Al/W mixture. The calculated flow stress of PTFE at a strain of 0.1 at the strain rate of 10^{-3} s^{-1} is approximately 10 MPa. This value is approximately one half of the value of the strength of the composite sample surrounded by 1.5 mm Al ring (Fig. 9), suggesting that the majority of the deformation takes place in the continuous PTFE matrix.

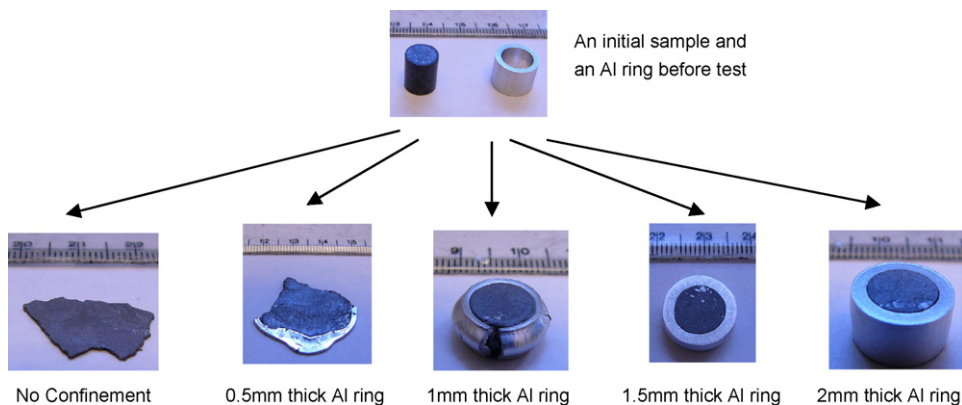


Fig. 5. Configuration of samples before (top) and after (bottom) testing.

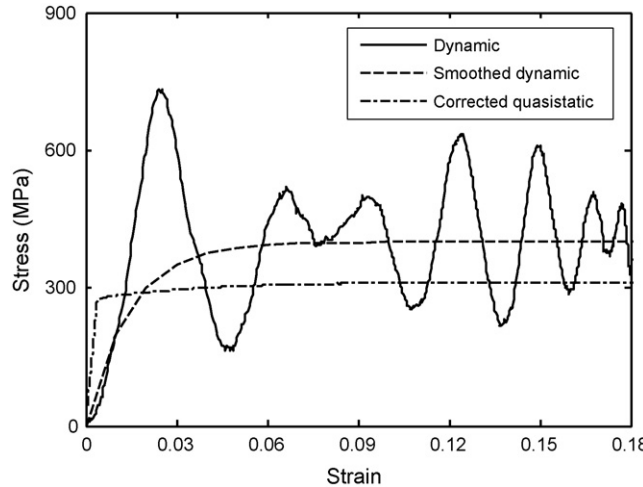


Fig. 6. Quasistatic and dynamic (drop-weight test) response of aluminum alloy used in sample confinement.

The addition of metal increased the flow stress (dashed curve in Fig. 8(b)). However, the strain-rate sensitivity is not changed. It is seen that the PTFE/Al/W mixture parallels the Z-A equation at low strains. Flow stresses of composites tested via the drop-weight apparatus are higher because of the confinement effect and the drop-weight technique itself.

The parameters for PTFE that were used in Z-A equation are shown in Table 1. Please note the values of ω_a and ω_p and the units of B_{pb} and B_{0pb} are different from Zerilli–Armstrong's. It can be seen that PTFE exhibits very high-strain-rate and temperature sensitivity (much higher than metals). This is a defining feature of polymers.

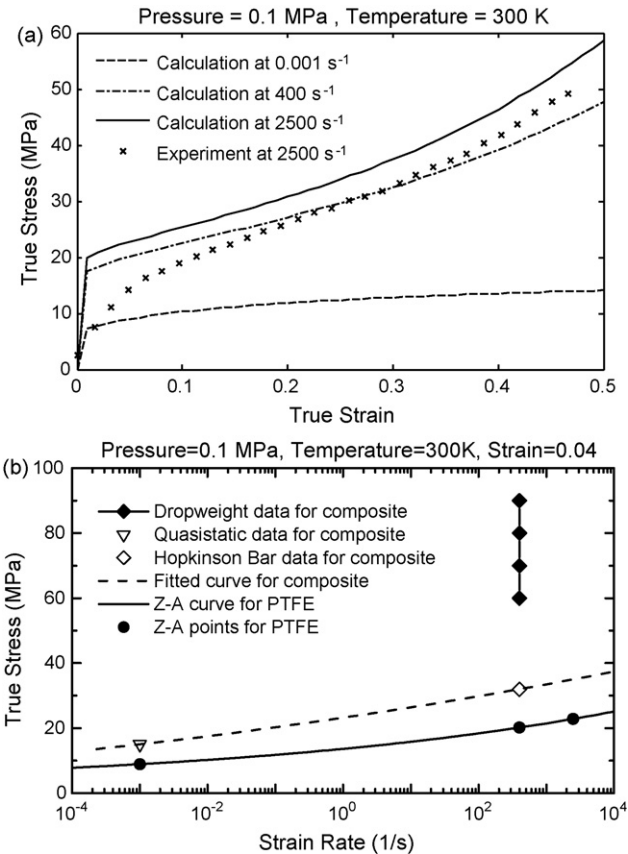


Fig. 8. (a) Experimental and computed compressive stress–strain curves of PTFE at different strain rates. (Experimental data adopted from Ref. [17]); (b) Comparison of composite PTFE/Al/W and PTFE on compressive strength at the same strain. (Hopkinson Bar data for composite were provided by Vecchio and Jiang [29]).

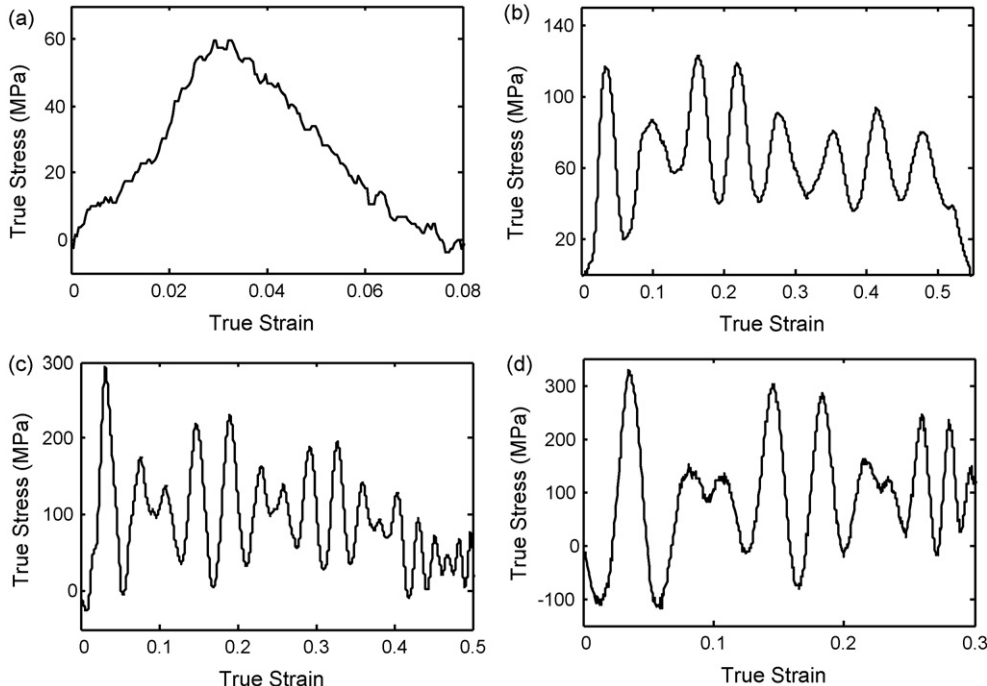


Fig. 7. Compressive response of samples subjected to various confinement conditions: (a) no confinement; (b) 0.5 mm Al; (c) 1 mm Al; (d) 1.5 mm Al.

Table 1

Parameters in Zerilli–Armstrong equation for the visco-plastic deformation of PTFE

β_0 (K^{-1})	2.01×10^{-2}
β_1 (K^{-1})	2.64×10^{-4}
α_0 (K^{-1})	4.78×10^{-3}
α_1 (K^{-1})	5.02×10^{-5}
ω_a	-2
ω_b	-0.625
ω_p (MPa $^{-1}$)	-3.1×10^{-2}
B_{pa} (MPa)	4016
B_{pb} (MPa $^{-1}$)	2.0×10^{-2}
B_{pn}	0.714
B_{0pa} (MPa)	72.4
B_{0pb} (MPa $^{-1}$)	2.2×10^{-2}
B_{0pn}	0.5

3.3. High-speed photography

This technique was used on an unconfined specimen to establish the degree of uniformity of deformation. The results are shown in the sequence of Fig. 10. This is a negative, i.e. the dark regions correspond to the outside and the light to the specimen and compression platens. The specimen position is marked SP. in Fig. 10. The initial height of the specimen, h_0 , was equal to 8 mm. Four snapshots are shown, at decreasing heights, h : 7, 6, 5, and 4 mm; they correspond to true compressive strains of -0.133, -0.288, -0.470, and -0.693. One of two lateral surfaces of the specimen (left surface) is shown. For $h = 7$ mm, the surface is fairly smooth. As the strain increases, irregularities at the surface initiate and grow. They are marked with arrows in Fig. 10(d). These irregularities are due to shear localization/cracking. It can be concluded that, in the absence of confinement, the deformation becomes highly heterogeneous. These results are consistent with the stress collapse measured in the unconfined compressive test (Fig. 7(a)).

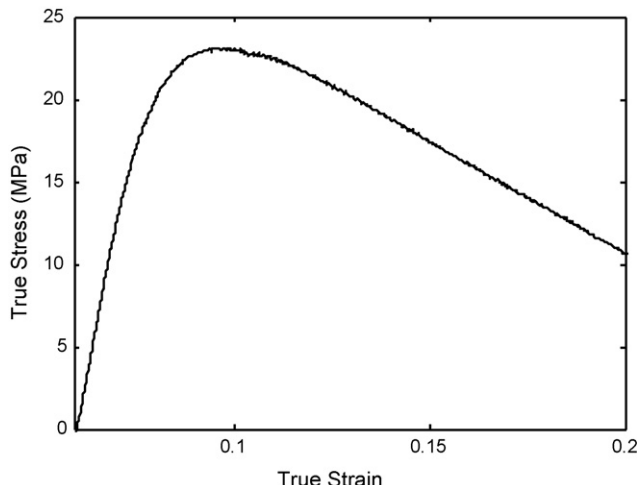


Fig. 9. Quasistatic compression response ($\dot{\varepsilon} \sim 10^{-2} s^{-1}$) of composite sample surrounded by 1.5 mm Al ring (force on ring subtracted from the total force).

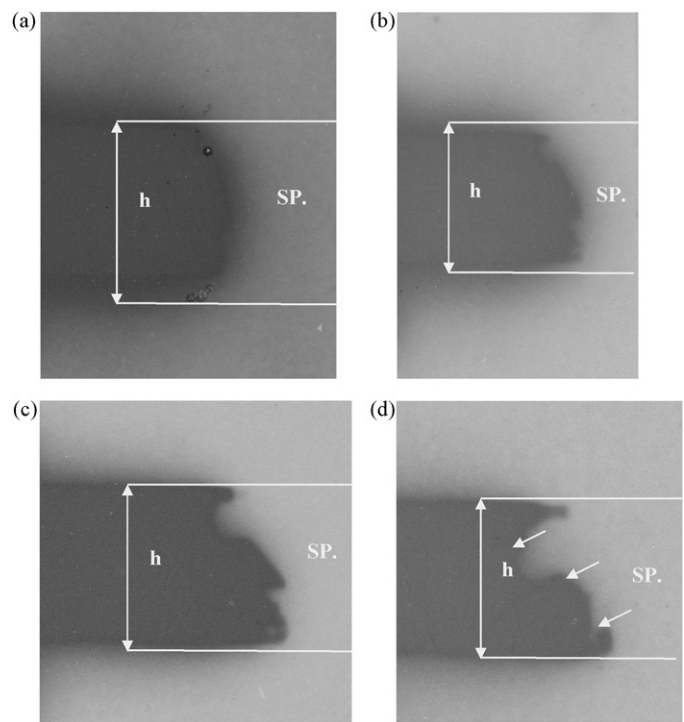


Fig. 10. Snapshots from high-speed photography of compression of unconfined specimen: (a) height = 7 mm, $\varepsilon = -0.133$; (b) height = 6 mm, $\varepsilon = -0.288$; (c) height = 5 mm, $\varepsilon = -0.470$; (d) height = 4 mm, $\varepsilon = -0.693$.

3.4. Microstructural evolution in plastic deformation

Specimens after different levels of plastic deformation were characterized by scanning electron microscopy to identify the failure mechanisms. Fig. 11 shows the top surface of a specimen deformed with the 2 mm Al ring confinement. A few cracks could be seen, and their observation enables the conclusion that failure starts at the W–PTFE/Al interfaces. Three areas where separation has started are indicated by arrows in Fig. 11. The

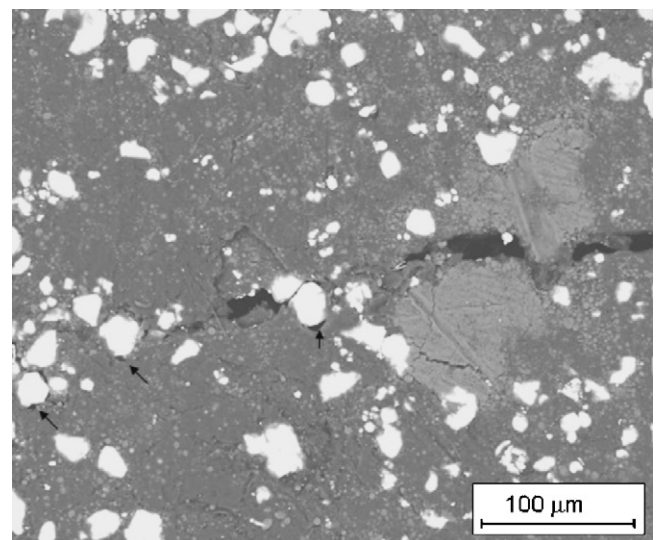


Fig. 11. Crack propagation through composite showing separation of W and PTFE interface (indicated by arrows).

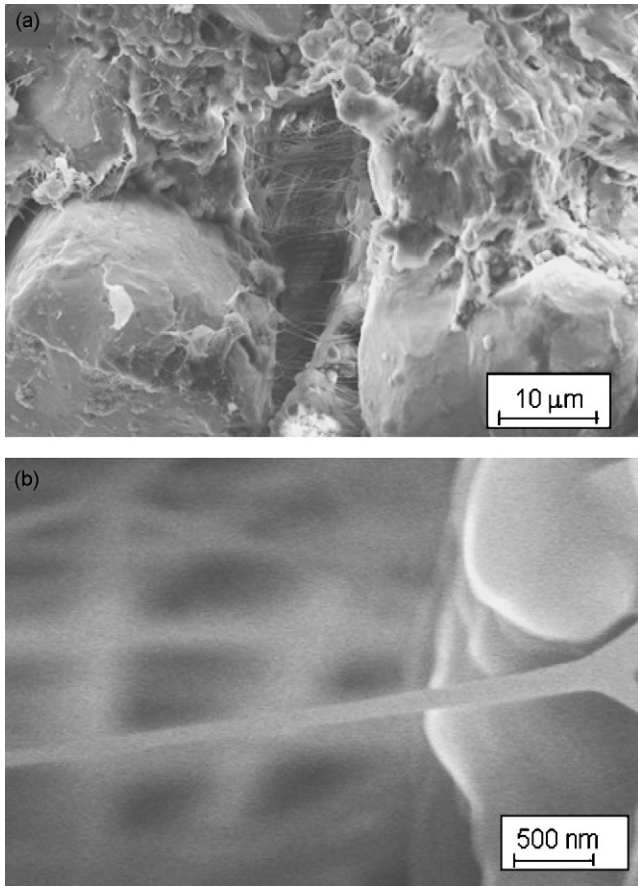


Fig. 12. PTFE fibers formed by opening crack: (a) overall view; (b) detail.

small ($2 \mu\text{m}$) Al particles are more clearly visible in Fig. 11 than in Fig. 3(b). Observation of a fracture surface (Fig. 4(a)) reveals three features: undeformed W particles, undeformed Al particles and highly deformed PTFE forming long strings in some places. In areas where large localized separation occurred, these strings form a dense network (Fig. 12(a)). A detailed view of one of these fibers is shown in Fig. 12(b). Their diameter is as low as 60–100 nm. In this sense, they can be termed nanofibers. A network of these PTFE nanofibers is also shown in Fig. 13. They are evidence of crazing. It has been observed by Brown et

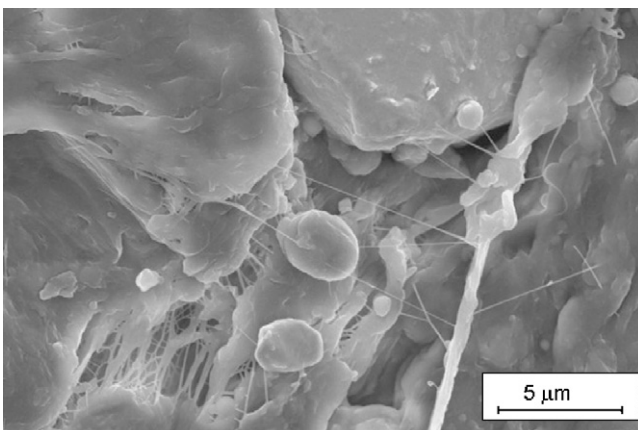


Fig. 13. Network of PTFE nanofibers formed along crack.

al. [28] that PTFE forms fibers when it is deformed at temperature above 30°C . The formation of these nanofibers is connected with the crazing phenomenon, with fibers providing additional resistance for a propagating crack. They are most likely the result of the heating of PTFE due to adiabatic deformation. This PTFE is bonded to the W particles in places and, upon fracture and separation of the W particles, is stretched in the same manner as chewing gum glued to two fingers that are pulled apart. The pressed but not sintered PTFE in the investigated composites deformed in a different fashion than the sintered PTFE when it was tested in Mode I fracture (tension specimens) [28]. The PTFE in our specimens was deformed with sparse fibers formation and considerable cleavage. The similar behavior was exhibited in Mode II (shear loading) fracture testing by Brown et al. [28]. It should be noticed that the PTFE fibers in our specimens are much thinner (60–100 nm) than the fibers ($\sim 1 \mu\text{m}$) in the experiments by Brown et al. [28]. It is possible that good thermal conduction of metal particles (W and Al) leads to faster cooling of deformed polymer, resulting in more marked crazing and fine fibers.

4. Conclusions

The high-strain, high-strain-rate experiments carried out on PTFE/Al/W granular composites with varying Al confinement rings reveal the characteristics of deformation and the strengths under high-strain rate ($\sim 4 \times 10^2 \text{ s}^{-1}$).

- The quasistatic flow stress is $\sim 22 \text{ MPa}$ and the dynamic flow stress is approximately 60–90 MPa. This is consistent with the constitutive description by Zerilli and Armstrong [25], assuming that deformation takes place mainly on the continuous PTFE matrix.
- In unconfined specimens, failure by cracking and shear localization follows immediately the maximum stress.
- Confinement with aluminum rings enables plastic deformation to continue to high values (up to a strain of -0.875).
- PTFE attached to W particles is extended in fracture, creating a network of new fibers having diameters as low as 60 nm.
- Most of the plastic deformation takes places in the “soft” PTFE, and the W particles remain virtually undeformed. It is this deformation that leads to the formation of the nanofibers.

Acknowledgements

We thank the US Office of Naval Research Award N00014-06-1-0263 (Dr. J. Goldwasser, Program Director) for support of this research program. Scanning electron microscopy was carried out with the assistance of Evelyn York (SIO) and Ryan Anderson (Cal IT²). Their help is greatly appreciated.

References

- [1] A.Y. Dolgoborodov, M.N. Makhov, I.V. Kolbanov, A.N. Streletskev, V.E. Fortov, *Jetp Lett.* 81 (2005) 311–314.

- [2] K. Choo, M.W. Baker, T.C.A. Molteno, S.W. Morris, Phys. Rev. E 58 (1998) 6115–6123.
- [3] J.M. Huntley, Philos. Trans. Roy. Soc. Lond. Series A 356 (1998) 2569–2590.
- [4] X. Xu, N.N. Thadhani, J. Appl. Phys. 96 (2004) 2000–2009.
- [5] N.N. Thadhani, J. Appl. Phys. 76 (1994) 2129–2138.
- [6] M.A. Meyers, L. Yu, K.S. Vecchio, Acta Metall. Mater. 42 (1994) 715–729.
- [7] K.S. Vecchio, L. Yu, M.A. Meyers, Acta Metall. Mater. 42 (1994) 701–714.
- [8] D.E. Eakins, N.N. Thadhani, J. Appl. Phys. 101 (2007) 043508.
- [9] N.K. Bourne, G.T. Gray, J. Appl. Phys. 98 (2005) 123503.
- [10] J.C.F. Millett, N.K. Bourne, J. Appl. Phys. 89 (2001) 2576–2579.
- [11] J.C.F. Millett, N.K. Bourne, J. Appl. Phys. 88 (2000) 7037–7040.
- [12] N.K. Bourne, J.C.F. Millett, G.T. Gray III, P. Mort, in: M.D. Furnish, N.N. Thadhani, Y. Horie (Eds.), Shock Compression of Condensed Matter 2001, American Institute of Physics, Melville, NY, 2002, pp. 653–656.
- [13] M.R. Baer, J. Appl. Mech. Trans. ASME 55 (1988) 36–43.
- [14] O.V. Roman, V.F. Nesterenko, I.M. Pikus, Combustion, Explosion, and Shock Waves (English Translation of Fizika Goreniya i Vzryva) March (1980) 644–649.
- [15] V.F. Nesterenko, Dynamics of Heterogeneous Materials, Springer-Verlag, New York, 2001.
- [16] D.L. Woody, J.J. Davis, P.J. Miller, in: T.B. Brill, T.P. Russell, W.C. Tao, R.B. Wardle (Eds.), Proceedings of the 1995 MRS Fall Symposium, Materials Research Society, Boston, MA, 1996, pp. 445–449.
- [17] S.M. Walley, J.E. Field, P.H. Pope, N.A. Safford, Philos. Trans. Roy. Soc. Lond. Series A 328 (1989) 1–33.
- [18] S.M. Walley, J.E. Balzer, W.G. Proud, J.E. Field, Proc. Roy. Soc. Lond. Series A 456 (2000) 1483–1503.
- [19] J.E. Field, Acc. Chem. Res. 25 (1992) 489–496.
- [20] S.M. Walley, P.D. Church, M. Furth, J.E. Field, J. De Phys. IV 7 (1997) 317–322.
- [21] K.R. Coleman, in: H. Schardin, O. Helwisch (Eds.), Proceedings of Forth Int. Kongress Kurzezeitphotographie, Darmstadt, Germany, 1959, pp. 32–39.
- [22] X.X. Yao, S. Zajac, Scand. J. Metall. 29 (2000) 101–107.
- [23] R.C. Picu, G. Vincze, F. Ozturk, J.J. Gracio, F. Barlat, A.M. Maniatty, Mater. Sci. Eng. A 390 (2005) 334–343.
- [24] M.F. Shi, D.J. Meuleman, J. Mater. Eng. Perform. 4 (1995) 321–333.
- [25] F.J. Zerilli, R.W. Armstrong, J. Phys. IV: JP 10 (2000) 3–8.
- [26] F.J. Zerilli, R.W. Armstrong, J. Appl. Phys. 61 (1987) 1816–1825.
- [27] F.J. Zerilli, R.W. Armstrong, J. Appl. Phys. 68 (1990) 1580–1591.
- [28] E.N. Brown, P.J. Rae, E.B. Orler, G.T. Gray, D.M. Dattelbaum, Mater. Sci. Eng. C 26 (2006) 1338–1343.
- [29] K.S. Vecchio, F. Jiang, unpublished results, 2007.